LRP 694/01 May 2001

# Neoclassical transport and α-particle confinement in novel 3D reactor systems

O. Fischer, W.A. Cooper, M.Yu. Isaev,
L. Villard

Submitted for publication in
Nuclear Fusion

ISSN 0458-5895

# Neoclassical transport and $\alpha$-particle confinement in novel 3D reactor systems

O. Fischer*, W.A. Cooper, M. Yu Isaev†, L. Villard

*Centre de Recherches en Physique des Plasmas, Association Euratom-Confédération Suisse, Ecole Polytechnique Fédérale de Lausanne, CRPP-PPB,CH-1015 Lausanne, Switzerland*

† *Russian Research Centre, Kurchatov Institute, Nuclear Fusion Institute, 123182 Moscow, Russia*

May 8, 2001

*E-mail: Olivier.Fischer@epfl.ch

**Abstract**

The study of neoclassical transport and $\alpha$-particle confinement is analysed in 3D reactor designs like the QAS3, the ST/sphellamak hybrid and the sphellamak using the VENUS code. We have observed that neither the QAS3 nor the ST/sphellamak are truly quasiaxisymmetric configurations. Thus the transport is governed by the helical deformation of the magnetic field strength and these configurations do not effectively confine the trapped $\alpha$-particles. On the other hand, the sphellamak is a nearly isodynamic structure in the plasma core which leads to almost perfect $\alpha$-confinement and the neoclassical transport is very similar to that obtained in a 2D equivalent tokamak.

# 1 Introduction

One of the main conditions that a fusion reactor should achieve is the confinement of $\alpha$-particles. In fact, it is necessary to keep the $\alpha$-particles during 0.1 $[s]$ inside the plasma so that they deposit their energy through collisional process within the plasma. Unlike tokamaks, fully 3D devices have a very poor level of $\alpha$-particle confinement due to the 3D structure of the magnetic field. However, during the last few years, a lot of progress has been realized in new 3D configurations with high performances of particle confinement such as the quasiaxisymmetric configurations, the quasi-isodynamic, the isodynamic structures or in a general context, the omnigenous systems.

New 3D configurations are presented as possible candidate for fusion reactors. We will focus our analysis on the effect of the 3D structure of the magnetic field strength on the $\alpha$-particle confinement as well as neoclassical diffusion of Deuterium ions. This is achieved with numerical calculations done by using the VENUS code [1] which solves the equations of the guiding centre drift orbits in Boozer coordinates [2, 3, 4] and estimates the diffusion coefficient [5].

The configurations studied are a quasiaxisymmetric stellarator with three field periods, the QAS3 [6], a hybrid design with features of a spherical tokamak, a tokamak and a stellarator, the ST/sphellamak hybrid [7] and finally the sphellamak [8]. The plasma parameters used for the simulations are of the same order as those in a nuclear reactor corresponding to a magnetic field strength on axis $B_{0,0}(0) \sim 5$ $[T]$, a plasma volume $V \sim 1000$ $[m^3]$ and $\beta \sim 5$ %. The QAS3 and the ST/sphellamak hybrid are studied by generating a sequence of configurations from a 2D equivalent tokamak to a fully 3D system. We have observed that these designs are not quasiaxisymmetric when the 3D features become important. This leads to a poor confinement for $\alpha$-particles and the diffusion coefficient is dominated by the effect of the helical deformation of the magnetic field. On the other hand, the sphellamak is a nearly isodynamic system in the plasma core which leads to a confinement and a neoclassical transport of the same order as that obtained in a 2D equivalent tokamak. Concerning the structure of this article, we give a brief review of the theory and describe the VENUS code in section 2. Then, the characteristics of the three designs are given in section 3. The numerical results are presented in section 4 and finally the discussion in section 5.

# 2 The Guiding Drift Orbit Equations and the Diffusion Coefficient

Boozer coordinates [2] have been used to evaluate the guiding centre drift orbits in fully 3D configurations. In these coordinates, the magnetic field in the contravariant form is described by $\mathbf{B}_0 = \nabla\psi(s) \times \nabla\vartheta + \nabla\zeta \times \nabla\chi(s)$ where $s = \psi(s)/\psi_{edge}$ while $\vartheta, \zeta, \psi$ and $\chi$ represent a poloidal coordinate, a toroidal coordinate, the toroidal flux function and the poloidal flux function, respectively. In the covariant form, $\mathbf{B}_0$ is given by $\mathbf{B}_0 = \mu_0 J(s)\nabla\vartheta - \mu_0 I(s)\nabla\zeta - \mu_0\nu(s,\vartheta,\zeta)\nabla s$, with $J$ and $I$ the toroidal and poloidal current flux functions, respectively and $\nu(s,\vartheta,\zeta)$ is a periodic function of $\vartheta$ and $\zeta$.

By introducing $q_e$ and $m_0$ the electronic charge and the rest mass of the particle, $E_p$ the particle energy, $\mu$ the magnetic moment and $\rho_{\|} = p_{\|}/(q_e B_0)$, the equations of the guiding centre motion are given by [2, 3, 4]

$$\dot{s} = \frac{\mu_0 I(s)}{D_b}\Big[(\frac{\mu}{q_e} + \frac{q_e B_0}{m_0}\rho_{\|}^2)\frac{\partial B_0}{\partial\vartheta}\Big] + \frac{\mu_0 J(s)}{D_b}\Big[(\frac{\mu}{q_e} + \frac{q_e B_0}{m_0}\rho_{\|}^2)\frac{\partial B_0}{\partial\zeta}\Big]\Big|_{(s,\vartheta,\zeta,t)}, \quad (1a)$$

$$\dot{\vartheta} = \frac{q_e B_0^2 \rho_{\|}}{m_0 D_b}\Big[\chi'(s) + \rho_{\|}\mu_0 I'(s)\Big] - \frac{\mu_0 I(s)}{D_b}(\frac{\mu}{q_e} + \frac{q_e B_0}{m_0}\rho_{\|}^2)\frac{\partial B_0}{\partial s}\Big|_{(s,\vartheta,\zeta,t)}, \quad (1b)$$

$$\dot{\zeta} = \frac{q_e B_0^2 \rho_{\|}}{m_0 D_b}\Big[\psi'(s) + \rho_{\|}\mu_0 J'(s)\Big] - \frac{\mu_0 J(s)}{D_b}(\frac{\mu}{q_e} + \frac{q_e B_0}{m_0}\rho_{\|}^2)\frac{\partial B_0}{\partial s}\Big|_{(s,\vartheta,\zeta,t)}, \quad (1c)$$

$$\begin{aligned}\dot{\rho}_{\|} = & -\frac{1}{D_b}\Big[\chi' + \rho_{\|}\mu_0 I'\Big]\Big[\frac{1}{\gamma}(\frac{\mu}{q_e} + \frac{q_e B_0}{m_0}\rho_{\|}^2)\frac{\partial B_0}{\partial\vartheta}\Big]\Big|_{(s,\vartheta,\zeta,t)} \\ & - \frac{1}{D_b}\Big[\psi' + \rho_{\|}\mu_0 J'\Big]\Big[\frac{1}{\gamma}(\frac{\mu}{q_e} + \frac{q_e B_0}{m_0}\rho_{\|}^2)\frac{\partial B_0}{\partial\zeta}\Big]\Big|_{(s,\vartheta,\zeta,t)} \\ & + \frac{\mu_0}{D_b}\Big[\frac{1}{\gamma}(\frac{\mu}{q_e} + \frac{q_e B_0}{m_0}\rho_{\|}^2)\frac{\partial B_0}{\partial s}\Big]\Big|_{(s,\vartheta,\zeta,t)}, \end{aligned} \quad (1d)$$

$$\rho_{\|} = \pm\frac{1}{q_e B_0}\sqrt{2m_0(E_p - \mu B_0)}\Big|_{(s,\vartheta,\zeta,t)} \text{ if } \partial E_p/\partial t = 0, \quad (1e)$$

where

$$D_b = \mu_0\Big[\chi'(s)J(s) - \psi'(s)I(s)\Big]\Big[1 + \mu_0\rho_{\|}\frac{J(s)I'(s) - I(s)J'(s)}{\chi'(s)J(s) - \psi'(s)I(s)}\Big].$$

Note that we can use Eq. (1e) instead of Eq. (1d) when the energy $E_p$ does not depend explicitly on time which is a consequence of the conservation of the energy.

The estimation of the diffusion coefficient is done by using Eq. (1a)-(1d) (or Eq. (1e)) and by applying a Lorentz scattering operator for the pitch angle at each time

step of the integration [5]. We change the pitch angle $\lambda = v_{||}/v$ from $\lambda_0$ to $\lambda_n$ after a time step of length $\tau$ with the formula $\lambda_n = \lambda_0(1 - \nu_d\tau) \pm \sqrt{(1-\lambda_0^2)\nu_d\tau}$ where $\nu_d$ is the deflection collision frequency defined in [9]. The symbol $\pm$ means the sign is to be chosen randomly. If the process is diffusive, the calculation of the dispersion $\sigma^2(t) =< (\Delta s(t))^2 > - < \Delta s(t) >^2$ with $\Delta s(t) = s(t) - s_0$ (typically $s_0 = 0.25$) allows to estimate the diffusion coefficient $D = \sigma^2(t)/2t \cdot a^2$ $[m^2/s]$ where $a$ is the minor radius as is mentioned in [10].

We have developed the **VENUS** code in order to solve the equations of motion defined by Eqs. (1a), (1b), (1c) and (1d) and to take into account the pitch angle scattering. It is a massively parallelized code written in Fortran 77 that uses the MPI library. The numerical tools used in the VENUS code consist of numerical interpolations and integrations. The interpolations are performed in a 2D $(s, \vartheta)$ plane (a four point method) and a quadratic interpolation in the $\zeta$ direction. The dimension of the array depends on the geometry studied and the memory size of the computer used for the simulation. But we have to be careful on the number of points in the $\vartheta$ direction because the poloidal coordinate spreads out on the low field side (LFS) in the Boozer coordinates. Concerning the numerical integrations, we have tested different methods: Runge-Kutta (RK) Merson variable-step (NAG library D02BGF) [11], Adams variable-order variable-step (NAG library D02CJF) [11], Symplectic RK [12], a fourth-order Runge Kutta (RK4) coupled with a second order Runge Kutta (RK2) with fixed time step. We have remarked that by using a variable-step, the computational time increases compared to a fixed time step due to the increasing number of calls to evaluate the right hand side of the ordinary differential equations (ODE). Consequently, we have decided to choose fixed time step methods. We can think that the Symplectic integrator is the best one for our case because the equations of motion are described by Hamilton equations. Unfortunately, the symplectic integrators are by definition completely implicit which causes a huge computational time. For these reasons, we have chosen a simple RK4 method for the integration of equation Eqs. (1a), (1b), (1c) and (1d). In the case of autonomous systems, $\partial E_p/\partial t = 0$, we know that $\rho_{||}$ can be evaluated by using Eq. (1e) and we reduce the dimension of the integration to three. This method can be applied directly to circulating particles for which $\rho_{||}$ does not change sign. But for trapped particles for which $\rho_{||}$ changes sign at the turning point, it is not possible to use this

method. Thus, we have developed a RK4 method coupled with a RK2 integrator. The principle consists in integrating Eqs. (1a), (1b), (1c) and (1d) from $t_0 \rightarrow t_1 = t_0 + \Delta t$ by using a RK2 approach. If $\rho_{\|}$ does not change sign, we repeat the integration from $t_0 \rightarrow t_1 = t_0 + \Delta t$ with a RK4 using Eqs. (1a), (1b), (1c) and (1e) for $\rho_{\|}$. Otherwise, we continue the integration with the RK2 until the particle reaches the turning point. This method is repeated at each time step. This scheme which conserves the energy $E_p$, requires five calls of the right hand side contrary to a RK4 method which needs four calls. Finally, the VENUS code can take a magnetic perturbation $\delta\mathbf{B}$ given by $\delta\mathbf{B} = \nabla \times (\Upsilon(s, \vartheta, \zeta)\mathbf{B}_0)$ into account as described in [4, 13].

To check the VENUS code, we have compared the lost collisionless $\alpha$-particles in a reactor design of W7X with the MCT code [14] (Fig. 1a) and with the VENUS code (Fig. 1b). The same behaviour for $\alpha$-confinement is observed. Concerning the diffusion coefficient, we have estimated $D$ for the TEXTOR tokamak with Deuterium ions with $E_p = 500\,[eV]$ by assuming that the bulk of ions have the same temperature as the particle energy ($E_p = T$) and compare the VENUS results with the GC3 code [15, 16] and with the standard formula given in [17, 10]. In Fig. 1c), we have plotted the analytic estimation of $D$ with the solid line, the squares are the VENUS results and the circles are the GC3 estimation versus frequency and we observe that the VENUS results are very close to the analytic prediction (less than 15%) and to the GC3 results.

# 3 The Configurations Investigated

## 3.1 The Quasiaxisymetric Stellarator with 3 Field Periods

The QAS3 (quasiaxisymmetric stellarator with 3 field periods) has been proposed by Garabedian and Ku in [6] as a possible candidate for a new stellarator in Princeton. We show in Fig. 2a) the magnetic field strength on the last closed flux surface (LCFS). Our purpose is to study a sequence from a 2D equivalent tokamak to the QAS3 by deforming the plasma boundary. This is done by introducing a parameter $T$, as shown in Table 1. The tokamak equivalent is achieved by imposing $T = 0$ and the QAS3 configuration corresponds to $T = 1$.

The equilibria have been computed with the fixed boundary VMEC code [18] by imposing for the LCFS the Fourier components $R_{mn}$, $Z_{mn}$ that describe the shape of the plasma in Table 1. The total plasma current is modified to guarantee that the maximum value of $\iota$ remains constant. The Boozer coordinates have been calculated with the TERPSICHORE code [19] with the appropriate normalization $C_{vol}$ and $B_{norm}$ in order to have a plasma volume of 1000 $[m^3]$ and a magnetic field strength $B_{0,0}(0) \sim 5[T]$. In fact, a QAS3 reactor design can be realized by multiplying the $R_{mn}$ and $Z_{mn}$ proposed in [6] by a factor $C_{vol} \sim 2.5$ and the Jacobian $\sqrt{g}$ by a factor $C_{vol}^3$. The magnetic field has to be multiplied by a factor $B_{norm} \sim 5$. Consequently, the toroidal flux by a factor $B_{norm} \cdot C_{vol}^2$ and the pressure and mass profiles by $B_{norm}^2$.

## 3.2 The Spherical Tokamak Sphellamak Hybrid

The ST/sphellamak (Spherical Tokamak) hybrid design [7] consists of features of a spherical tokamak, a tokamak and a stellarator. This system is proposed to test whether helical coils can provide a fraction of the rotational transform and correspondingly reduce the current in the central conductor. This could alleviate problems with recirculating power inherent in ST devices. Moreover, shielding of the central core in a ST remains a rather intractable problem.

The ST/sphellamak design consists of 10 toroidal coils (TC) wound on a spherical structure of 1.1$[m]$ radius (Fig. 2b). Inside the TC, 10 modular helical Furth-Hartman type coils (HC) are wound on a sphere of 1 $[m]$. Moreover, there are 2 vertical field

| m | n/L | $R_{mn}\,[m]$ | $Z_{mn}\,[m]$ | m | n/L | $R_{mn}\,[m]$ | $Z_{mn}\,[m]$ |
|---|---|---|---|---|---|---|---|
| 0 | 0 | 3.50 | 0.00 | 1 | 3 | $0.02T$ | $-0.02T$ |
| 0 | 1 | $0.10T$ | $0.10T$ | 2 | 0 | 0.18 | 0.00 |
| 0 | 2 | $-0.01T$ | $0.01T$ | 2 | 1 | $0.12T$ | $0.18T$ |
| 1 | -2 | $-0.02T$ | $-0.02T$ | 2 | 2 | $0.06T$ | $-0.05T$ |
| 1 | -1 | $0.02T$ | 0.00 | 3 | -1 | $0.01T$ | $-0.01T$ |
| 1 | 0 | 0.70 | 1.30 | 3 | 0 | -0.02 | 0.02 |
| 1 | 1 | $-0.30T$ | $0.30T$ | 3 | 1 | $0.02T$ | $-0.02T$ |
| 1 | 2 | $0.04T$ | $-0.04T$ | 3 | 3 | $-0.02T$ | $0.02T$ |

Table 1: Fourier decomposition of the boundary of QAS3 configuration. $T$ varies from 0 to 1. The reactor design is achieved by multiplying the $R_{mn}$ and the $Z_{mn}$ by a factor $C_{vol} \sim 2.5$.

coils (VF) in the polar region which compensate the current flowing in the toroidal arc segments. Two other VF are localized near the mid-plane to control the plasma position. By changing the current flowing in the helical coils, we are able to modify the magnetic field structure from a 2D to a 3D configuration. In Table 2, we show the main parameters of the two configurations studied. The ST/sphellamak 1 is very close to a ST configuration while ST/sphellamak 4 is a fully 3D configuration.

We first compute equilibria with the free boundary VMEC code with the parameters described in Table 2. Then, the $R_{mn}$, $Z_{mn}$ of the LCFS and $B$ are multiplied by a factor of ten and are used in the fixed boundary VMEC code in order to reproduce the same features for all cases. Typically, we have imposed the $\iota$-profile, $\iota(s) = 1 - 2/3 \cdot s$ and a $\beta$ value of approximately 5.90 % is achieved. The TERPSICHORE code has been used in order to determine the Boozer coordinates.

| CONFIGURATION | $B_{00}\,[T]$ | $I_{hc}\,[kA]$ | $\beta\,\%$ | $R\,[m]$ | $a\,[m]$ |
|---|---|---|---|---|---|
| ST/sphellamak 1 | 0.497 | 20 | 5.90 | 0.666 | 0.308 |
| ST/sphellamak 4 | 0.473 | 180 | 5.88 | 0.702 | 0.321 |

Table 2: Characteristics of the ST/sphellamak hybrid device. The reactor design is achieved by multiplying $B_{0,0}, R$ and $a$ by a factor of ten.

## 3.3 The Sphellamak Design

A new design of sphellamak is proposed and analyzed [20, 8] which is a coreless hybrid system with spheromak, spherical tokamak and stellarator features. It consists in removing the toroidal coils of the ST/sphellamak hybrid (section 4.2) and leads to a real 3D configuration. The absence of a central conductor permits the potential realization of a very compact design because the shielding becomes unnecessary. The vacuum magnetic field is produced by only the ten helical Furth-Hartman coils and the vertical field coils. A view of the coil geometry is plotted in Fig. 2c) with the last closed flux surface inside the coils. Now depending on the current flowing in the helical coils, we are able to modify the $B$ structure. Consequently, a study has been realized by varying the helical current $I_{hc}$ from $42\,[MA] < I_{hc} < 122\,[MA]$ ($I_{hc,1} = 122$, $I_{hc,2} = 102$, $I_{hc,3} = 82$, $I_{hc,4} = 62$, $I_{hc,5} = 42\,[MA]$). The equilibria have been computed with the free boundary VMEC code by imposing a peaked toroidal current profile $J'(s) = J'_0[3(1-s)^5 + (1-s^5)^2]/4$, a pressure profile $p(s) = p_{0,i}(1-s^2)^2$ with $p_{0,i}$ chosen in order to maintain a $\beta = 7.3\,\%$ value for all the configurations and a plasma current $I_p = 30\,[MA]$. The plasma volume $V$ and the magnetic field depend on the value of $I_{hc}$. In fact, by increasing $I_{hc}$, the magnetic field increases ($B^2_{0,0} \sim 25\,[T^2] \rightarrow 40\,[T^2]$) while the volume decreases ($V \sim 700\,[m^3] \rightarrow 500\,[m^3]$) which is favorable for particle confinement, because low volume corresponds to high magnetic field in the sequence explored. All equilibrium parameters are displayed in Table 3. Finally, the Boozer coordinates have been determined with the TERPSICHORE code.

| CONFIGURATION | $B^2_{00}\,[T^2]$ | $I_{hc}\,[MA]$ | $\beta\,\%$ | $R\,[m]$ | $a\,[m]$ | $V\,[m^3]$ |
|---|---|---|---|---|---|---|
| sphellamak 1 | 41.50 | 122 | 7.33 | 4.66 | 2.28 | 480 |
| sphellamak 2 | 37.40 | 102 | 7.24 | 4.62 | 2.37 | 515 |
| sphellamak 3 | 33.37 | 82 | 7.31 | 4.60 | 2.48 | 561 |
| sphellamak 4 | 29.65 | 62 | 7.29 | 4.60 | 2.61 | 621 |
| sphellamak 5 | 26.33 | 42 | 7.29 | 4.64 | 2.76 | 702 |

Table 3: Characteristics of the sphellamak device.

# 4 Numerical Results

## 4.1 The QAS3 Configuration

By comparing the Fourier components of the two limiting configurations $T = 0$ and $T = 1$, we see as expected that with $T = 0$, the QAS3 is a tokamak configuration (Fig. 3a). But by fixing $T = 1$, the behaviour of $B^2_{mn}$ is totally different. We see in Fig. 3b) that $B^2_{0,0}$ apart (also its value on axis has been subtracted), the two most important amplitudes are $B^2_{1,0}$ and $B^2_{0,3}$. The first one indicates that a quasiaxisymmetric configuration is achieved which leads to good confinement properties. But on the other hand, the $B^2_{0,3}$ component yields a mirror effect which causes a degradation of confinement as trapped particles should leave the plasma very fast.

In fact, if we analyze the $\alpha$-collisionless particles in such a device (14000 particles have been used with $s_0 = 0.25$), we observe in Fig. 3c) that an increase of $T$ leads to an increase of particles lost (most of them are trapped particles) due to the presence of the mirror field term. The time that trapped particles leave the plasma, $T_{lost}$, is approximatively $T_{lost} \sim 1\,[ms]$ which is much less than the energy slowing-down time $\tau_\alpha \sim 0.1\,[s]$.

Now, if we examine the behaviour of the diffusion coefficient $D$ (5000 Deuterium ions used with $E_p = T = 10\,[keV]$) in Fig. 3d), we see that as expected, the $T = 0$ case shows a tokamak diffusion ($D$ is proportional the density), but when $T$ increases, we observe that $D$ becomes proportional to $1/n$ even with a small value of $T$ which means that the diffusion coefficient is governed by the helical magnetic field and $D$ increases by a factor six compared with the equivalent tokamak. To conclude, we can say that the QAS3 seems to be a 3D configuration with no symmetric properties and the transport is governed by the 3D features.

## 4.2 The ST/Sphellamak Hybrid Design

Of course the ST/sphellamak 1 is comparable to a tokamak device and only the $B^2_{m,n=0}$ amplitudes are important (shown in Fig. 4a) while the ST/sphellamak 4 seems to be a quasiaxisymmetric configuration, because the main component after the $B^2_{0,0}$ term is the $B^2_{1,0}$ contribution (Fig. 4b). Unfortunately, by looking Fig. 4c), we observe that the ST/sphellamak 4 possesses smaller components of $B^2_{m,10}$ that constitute non

negligible contributions. These annihilate the quasiaxisymmetric conditions which generates local ripples which cause a degradation of confinement for trapped particles. Moreover, by plotting in Fig. 4d) constant $J_{||}$ ($J_{||}$ is the second adiabatic invariant) contours in polar coordinates $(s, \vartheta)$ for the ST/sphellamak 4, we remark that they do not form closed surfaces. Closed $J_{||}$ contours characterise systems that are referred to as quasi-isodynamic [21] which satisfy a good confinement of particles despite a fully 3D structure of the $B$-field spectrum, because the particles do not drift far from their initial flux surfaces. Thus, the ST/sphellamak does not display a quasi-isodynamic structure. Finally, we note that the magnetic field strength has a typical $1/r$ dependence as shown in [7].

In Fig. 5a), we have plotted the lost $\alpha$-collisionless particle (5000 particles launched at $s_0 = 0.25$) percentage versus time and we see that the ST/sphellamak 1 confined all the particles perfectly contrary to ST/sphellamak 4 for which 10 % (most of them are trapped particles) are lost after a short time $T_{lost} \sim 1\ [ms]$ due to the magnetic field line ripple effects and the non quasi-isodynamic structure.

Concerning the diffusion coefficient, we have plotted in Fig. 5b) the behaviour of $D$ versus the density (5000 Deuteriums ions with $E_p = T = 10\ [keV]$ have been used). As we can observe, $D$ increases as a function of density for the ST/sphellamak 1 contrary to the ST/sphellamak 4 for which $D$ decreases. The reason is that for these parameters (density, temperature, etc.), we are in the low collisionality and the theory of neoclassical transport in stellarators [16, 22] predicts that $D \sim 1/n$ which is displayed by the solid line Fig. 5b). Moreover, there is a factor of one hundred between the diffusion coefficient of the ST/sphellamak 1 and the ST/sphellamak 4 which is enormous and of course a consequence of the ripple effect.

## 4.3 The Sphellamak Device

By analyzing the Fourier components of the sphellamak 1 in Fig. 6a), we remark that the spectrum is very close to a quasiaxisymmetric system and the amplitudes are comparable to the ST/sphellamak 4 shown in Fig. 4b). By examing smaller amplitudes, like the $B^2_{m,10}$ (Fig. 6b), we observe that they are non negligible and they are of the same order as the hybrid ST/sphellamak 4 case (Fig. 4c). By decreasing the current $I_{hc}$, the spectrum does not change except for the $B^2_{m,10}$ modes which are plotted in Fig. 6c). But the main difference between the ST/sphellamak hybrid and

the sphellamak is the global structure of the magnetic field. In fact, if we examine in Fig. 6d) constant $J_{||}$ contours for the sphellamak 1, we can conclude that the system is a nearly quasi-isodynamic structure contrary to the ST/sphellamak 4. Moreover, in [8], it is shown that the sphellamak displays isodynamic features in the plasma core. This yields a very high level of particle confinement.

As previously, we have estimated the loss of collisionless $\alpha$-particles for the five configurations. As we said, the nearly isodynamic structure near the central core of the plasma should lead in principle to good confinement. In fact, we have observed that only the configuration with $I_{hc,1} = 122\,[MA]$ yields a particle loss of approximatively 2 %, which is acceptable (Fig. 7a). Note that we have used 7500 particles for the simulations. All the other configurations perfectly confine all particles, as had been found in the tokamak device studied in this article shown in Fig. 3c) and in Fig. 5c). This is a consequence of the near isodynamicity of the system.

Concerning the neoclassical transport, we have plotted the diffusion coefficient in Fig. 7b) (6000 Deuterium ions with $E_p = T = 10\,[keV]$ have been used) for the five configurations (solid lines) and we have added the results obtained with the ST/sphellamak 1 and 4 (dashed lines). Expect for the sphellamak 1 and 2 cases, we remark that $D$ is of the same order as in an equivalent tokamak diffusion as shown by the pentagrams (dashed line) and any 3D behaviour of the magnetic field structure plays a negligible role. But the amplitude of the diffusion coefficient for the sphellamak 1 case is comparable to the ST/sphellamak 4 (dashed line with diamonds). The reason is probably due to the very similar behaviour for the Fourier components of $B^2$ for these two devices as was noted previously where the 3D effects of $B^2$ become important.

Finally, we have compared the VENUS results with the MCT code [14] for the loss of collisionless $\alpha$-particles in the two limited configurations, namely the sphellamak 1 and the sphellamak 5, shown in Fig. 8a) and Fig. 8b). As we can observe, the results are in good agreement as obtained previously in Fig. 7a) with the VENUS code.

# 5 Conclusions

The study of $\alpha$-particle confinement and the neoclassical transport in 3D configurations have been undertaken for three reactor devices using the VENUS code. The first design explored was the QAS3 which seems to have poor confinement properties when the 3D structure becomes non negligible. We have observed an increase of $\alpha$-particles lost due to the presence of a mirror field effect and the diffusion is governed by the nonsymmetric helical field structure. Secondly, the ST/sphellamak hybrid design and the sphellamak have been analyzed. The first one has shown, like in the QAS3, low confinement properties and a $1/n$ dependence on the diffusion has been observed. Even with small 3D deformations, local ripples appear in $B$ which are due to small but finite Fourier components and thus the system ceases to be quasiaxisymmetric. On the other hand, by removing the toroidal coils which yields the sphellamak concept, very different properties of confinement have been observed. In fact, the magnetic structure seems to acquire isodynamic features very different from the ST/sphellamak hybrid. We have shown that collisionless $\alpha$-particles are perfectly confined making it comparable to results obtained in 2D configurations like the tokamak even with a small plasma volume. Moreover, the amplitude of the diffusion coefficient is very similar to that obtained in a 2D equivalent tokamak.

To conclude, we can say that the sphellamak device appears to be a viable candidate as power producing reactor: very high level of collisionless $\alpha$-particle confinement and a low value for the diffusion coefficient under some conditions. This is a consequence of the near isodynamic structure of $B$ near the core which is closely linked with the quasi-isodynamic features that we have identified.


## ACKNOWLEDGMENTS

We thank Dr. S. P. Hirshman for providing us with the VMEC code and Dr. H. Mynick for providing us with the GC3 code. The computations have been performed on the Origin2000 of the EPFL. This work was partially sponsored by the Fonds National Suisse de la Recherche Scientifique and by Euratom.

# References


[1] O. Fischer, W. A. Cooper, M. Y. Isaev, and L. Villard, *Theory of Fusion Plasmas, Int. Workshop, Varenna* (Editrici Compositori, Società Italiana di Fisica, Bologna, 2000).

[2] A. H. Boozer, Phys. Fluids **23**, 904 (1980).

[3] W. A. Cooper, Plasma Phys. and Cont. Fusion **39**, 931 (1997).

[4] R. B. White and M. S. Chance, Phys. Fluids **27**, 2455 (1984).

[5] A. H. Boozer and G. Kuo-Petravic, Phys. Fluids **24**, 851 (1981).

[6] P. R. Garabedian and L. P. Ku, Phys. Plasmas **6**, 645 (1999).

[7] W. A. Cooper *et al.*, Plasma Phys. and Cont. Fusion **42**, 1105 (2000).

[8] W. A. Cooper and O. Fischer, EPFL Supercomputing Review **12**, 22 (2000).

[9] E. Strumberger, Nuclear Fusion **40**, 1697 (2000).

[10] R. H. Fowler, J. A. Rome, and J. F. Lyon, Phys. Fluids **28**, 338 (1985).

[11] N. L. Mark, *The NAG Fortran Libary, Mark 15* (NAG, Oxford, 1991).

[12] J. M. Sanz-Serna and M. P. Calvo, *Numerical Hamiltonian Problems* (Applied Mathematics and Mathematical Computation 7, Chapman & Hall, 1994).

[13] O. Fischer, W. A. Cooper, and L. Villard, Nuclear Fusion **40**, 1453 (2000).

[14] S. Gori, W. Lotz, and J. Nührenberg, *Theory of Fusion Plasmas, Int. Workshop, Varenna* (Editrici Compositori, Società Italiana di Fisica, Bologna, 1996).

[15] H. E. Mynick, Phys. Fluids **25**, 325 (1982).

[16] H. E. Mynick, Plasma Phys. Reports **23**, 547 (1997).

[17] F. L. Hinton and R. D. Hazeltine, Reviews of Modern Phys. **48**, 239 (1976).

[18] S. P. Hirshman, W. I. V. Rij, and P. Merkel, Comp. Phys. Comm. **43**, 143 (1986).

[19] D. V. Anderson *et al.*, The Int. Journal of Supercomputer Applications **4**, 34 (1990).

[20] W. A. Cooper, J. M. Antonietti, and T. N. Todd, *Proc. 17th IAEA Fusion Energy Conf.* (IAEA, Yokohama, Japan, 1998).

[21] S. Gori and J. Nührenberg, *Theory of Fusion Plasmas, Int. Workshop, Varenna* (Editrici Compositori, Società Italiana di Fisica, Bologna, 1998).

[22] K. Miyamoto, *Plasma Physics for Nuclear Fusion* (MIT Press, London, 1989).

## CAPTIONS

1. a) Percentage of lost collisionless $\alpha$-particles in a reactor design of W7X estimated by the MCT code versus time (top left) and b) by the VENUS code (top right). c) $D$ estimated by the GC3 code (circles), by the VENUS code (squares) and the analytic estimation (solid line) in the TEXTOR tokamak (bottom).

2. a) The $B$ contours in Boozer coordinates for the QAS3 with $T = 1$ on the LCFS (top). b) The ST/sphellamak hybrid is composed of ten toroidal coils, four verticals field coils and ten helical Furth-Hartman type coils (bottom left). c) The sphellamak design and the contour of $B$ on the LCFS (bottom right).

3. a) The Fourier amplitude profiles of $B^2_{mn}$ for the QAS3 with $T = 0$ (top left) and b) with $T = 1$ (top right) (Circles: $B^2_{0,0} - B^2_{0,0}(0)$. Squares: $B^2_{1,0}$. Stars: $B^2_{2,0}$. Triangles: $B^2_{3,0}$. Diamonds: $B^2_{0,3}$. Left triangles: $B^2_{1,3}$). c) Percentage of lost collisionless $\alpha$-particles in QAS3 (Circles: $T = 0$. Squares: $T = 0.25$. Triangles: $T = 0.5$. Stars: $T = 1$) (bottom left). d) Diffusion coefficient for Deuterium ions with $E_p = T = 10[keV]$ versus density (Squares: $T = 0$. Circles: $T = 0.25$. Stars: $T = 0.5$. Triangles: $T = 0.7$. Squares: $T = 0.8$. Diamonds: $T = 1$) (bottom right).

4. a) $B^2_{mn}$ in ST/sphellamak 1 (top left) and b) $B^2_{mn}$ in ST/sphellamak 4 (top right) (Circles: $B^2_{0,0} - B^2_{0,0}(0)$. Squares: $B^2_{1,0}$. Stars: $B^2_{2,0}$. Diamonds: $B^2_{0,10}$. Hexagrams: $B^2_{1,10}$). c) $B^2_{m,10}$ in ST/sphellamak 4 (Circles: $m = 0$. Squares: $m = 1$. Stars: $m = 2$. Diamonds: $m = 3$. Pentagrams: $m = 4$. Hexagrams: $m = 5$. Triangles: $m = 6$) (bottom left). d) Constant $J_{||}$-contours in polar-coordinates $(s, \vartheta)$ for ST/sphellamak 4 (bottom right).

5. a) Percentage of lost collisionless $\alpha$-particles in ST/sphellamak 1 and in ST/sphellamak 4 reactor design versus time (left). b) Diffusion coefficient for Deuterium ions with $E_p = T = 10\,[keV]$ in ST/sphellamak 1 (squares) and in ST/sphellamak 4 (diamonds) reactor design versus density (right). The solid line shows the behaviour when $D \sim 1/n$.

6. a) $B^2_{mn}$ for the sphellamak 1 (Circles: $B^2_{0,0} - B^2_{0,0}(0)$. Squares: $B^2_{1,0}$. Stars: $B^2_{2,0}$. Diamonds: $B^2_{0,10}$. Hexagrams: $B^2_{1,10}$) (top left). b) $B^2_{m,10}$ for the sphellamak 1

(top right) and c) for the sphellamak 5 (bottom left) (Circles: $m = 0$. Squares: $m = 1$. Stars: $m = 2$. Diamonds: $m = 3$. Pentagrams: $m = 4$. Hexagrams: $m = 5$. Triangles: $m = 6$). d) Constant $J_{||}$-contours in polar-coordinates $(s, \vartheta)$ for the sphellamak 1 (bottom right).

7. a) Percentage of lost collisionless $\alpha$-particles in sphellamak 1 (Circles) and sphellamak 5 (Squares) (left). b) Diffusion coefficient for Deuterium ions with $E_p = T = 10[keV]$ in sphellamak 1 to 5 and in ST/sphellamak 1 and 4 (Squares: $I_{hc} = 122$. Circles: $I_{hc} = 102$. Stars: $I_{hc} = 82$. Triangles: $I_{hc} = 62$. Inverted triangles: $I_{hc} = 42$. Pentagrams: ST/sphellamak 1 hybrid. Diamonds: ST/sphellamak 4 hybrid) (right).

8. a) MCT code calculations of lost $\alpha$-collisionless particles in sphellamak 1 (left) and b) in sphellamak 5 (right). Two different flux surfaces have been used, namely $s = 0.24$ and $s = 0.06$.

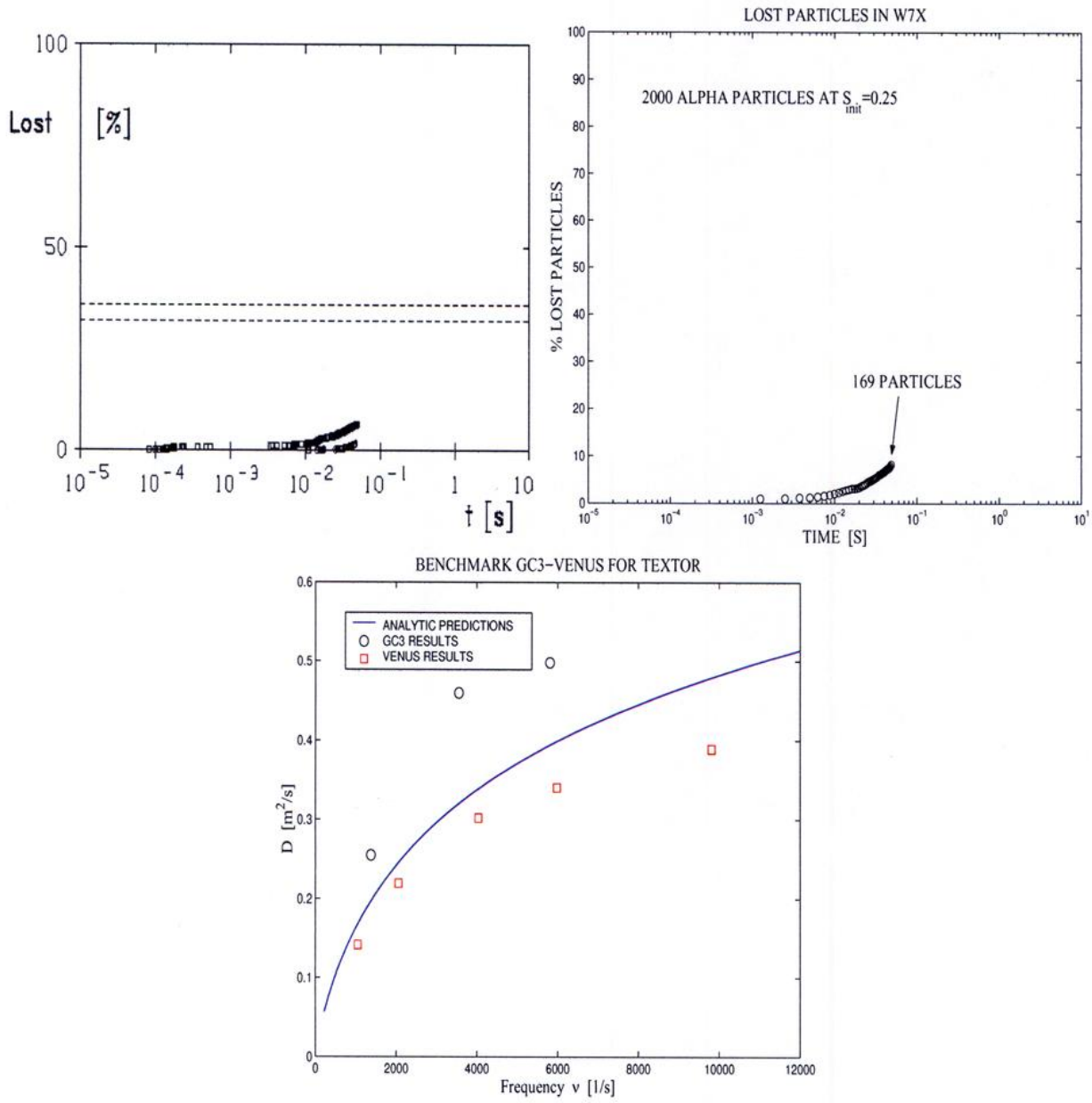
Lost [%]
100
50
0
10^-5 10^-4 10^-3 10^-2 10^-1 1 10
t [s]
LOST PARTICLES IN W7X
2000 ALPHA PARTICLES AT S_init=0.25
% LOST PARTICLES
169 PARTICLES
TIME [S]
BENCHMARK GC3-VENUS FOR TEXTOR
ANALYTIC PREDICTIONS
GC3 RESULTS
VENUS RESULTS
D [m^2/s]
Frequency ν [1/s]
0 2000 4000 6000 8000 10000 12000

Figure 1:

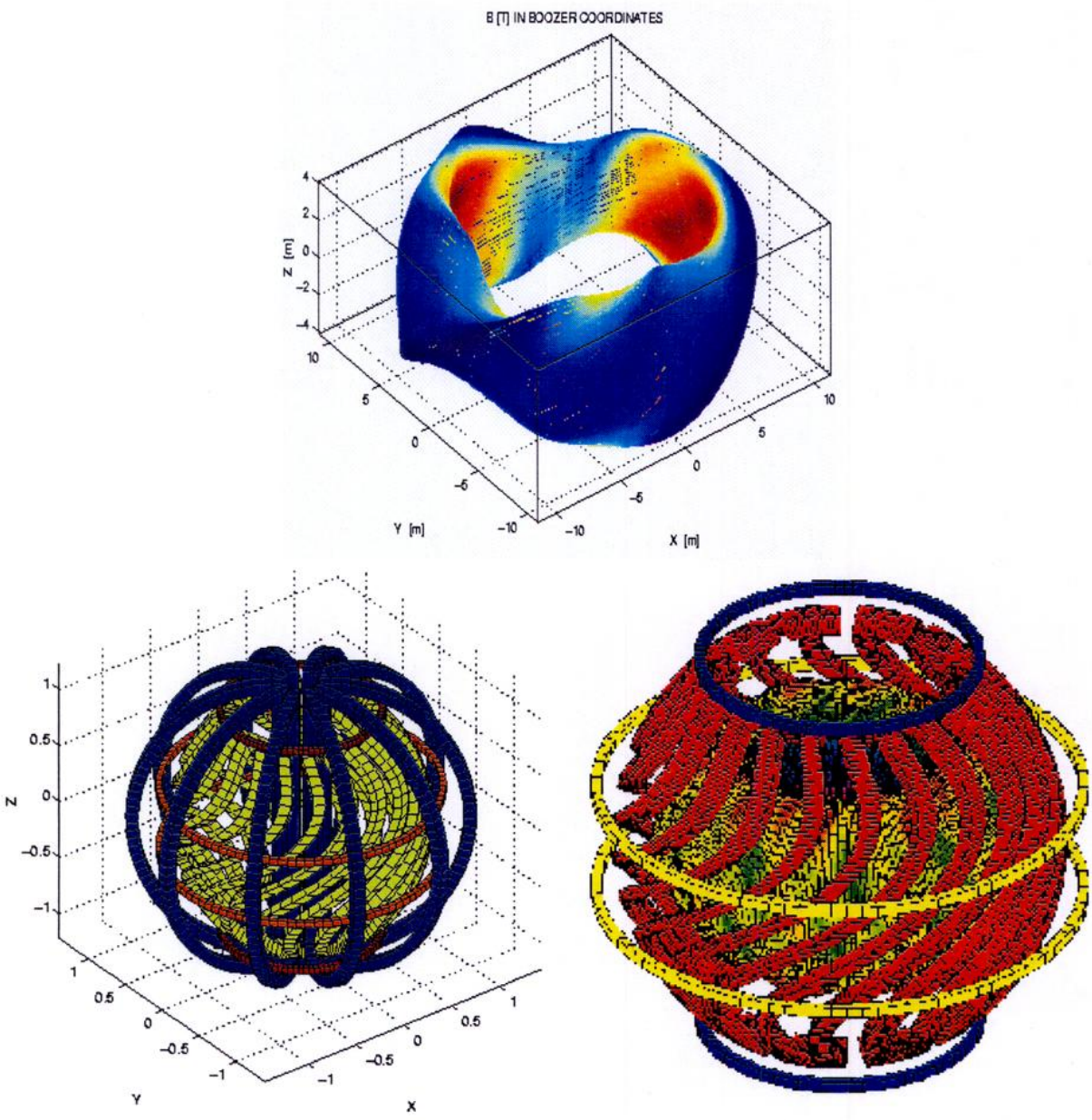


Figure 2:

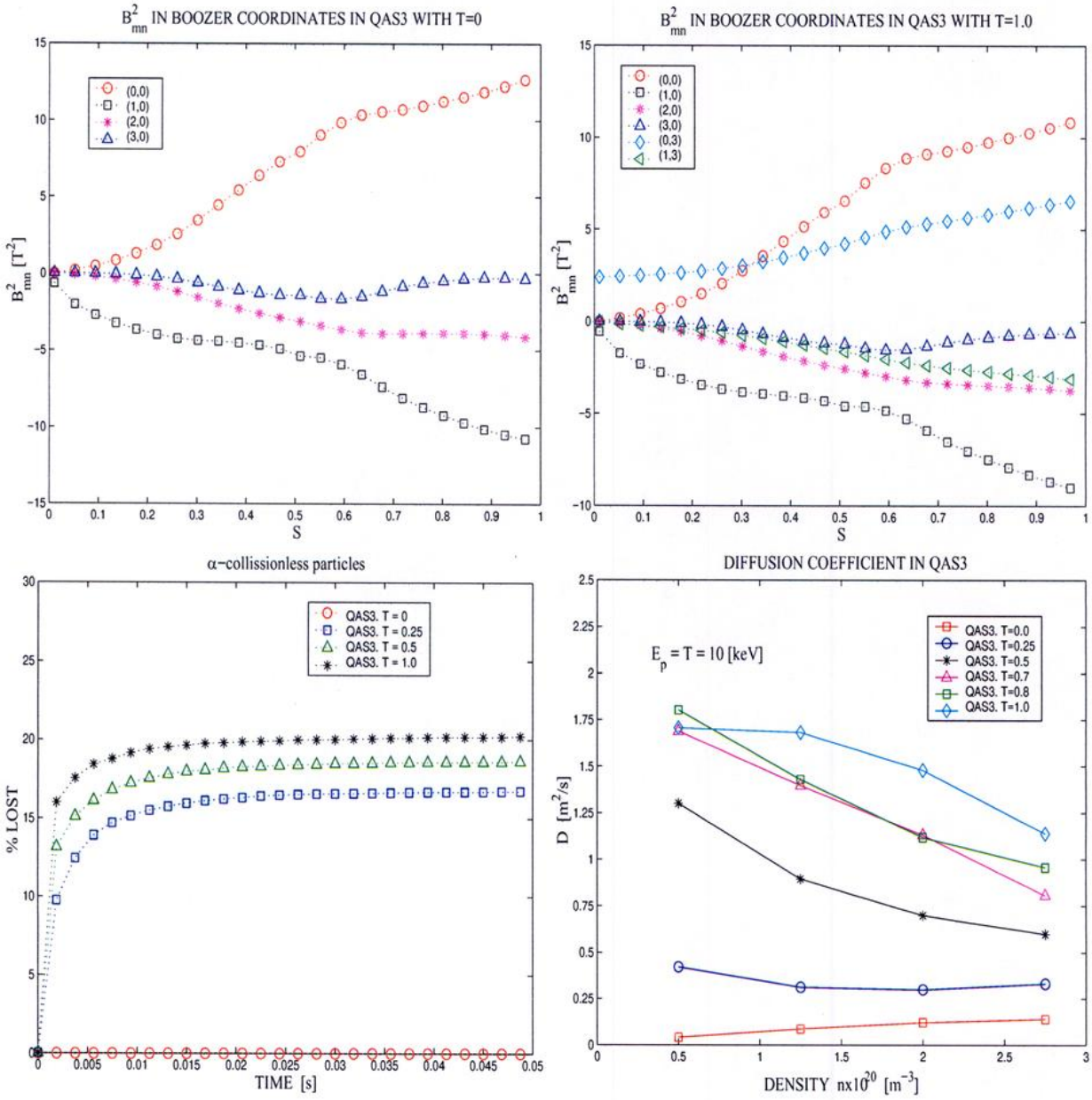
$B^2_{mn}$ IN BOOZER COORDINATES IN QAS3 WITH T=0
(0,0)
(1,0)
(2,0)
(3,0)
$B^2_{mn}$ [$T^2$]
S
$B^2_{mn}$ IN BOOZER COORDINATES IN QAS3 WITH T=1.0
(0,0)
(1,0)
(2,0)
(3,0)
(0,3)
(1,3)
$B^2_{mn}$ [$T^2$]
S
α−collissionless particles
QAS3. T = 0
QAS3. T = 0.25
QAS3. T = 0.5
QAS3. T = 1.0
% LOST
TIME [s]
DIFFUSION COEFFICIENT IN QAS3
$E_p$ = T = 10 [keV]
QAS3. T=0.0
QAS3. T=0.25
QAS3. T=0.5
QAS3. T=0.7
QAS3. T=0.8
QAS3. T=1.0
D [$m^2/s$]
DENSITY nx$10^{20}$ [$m^{-3}$]

Figure 3:

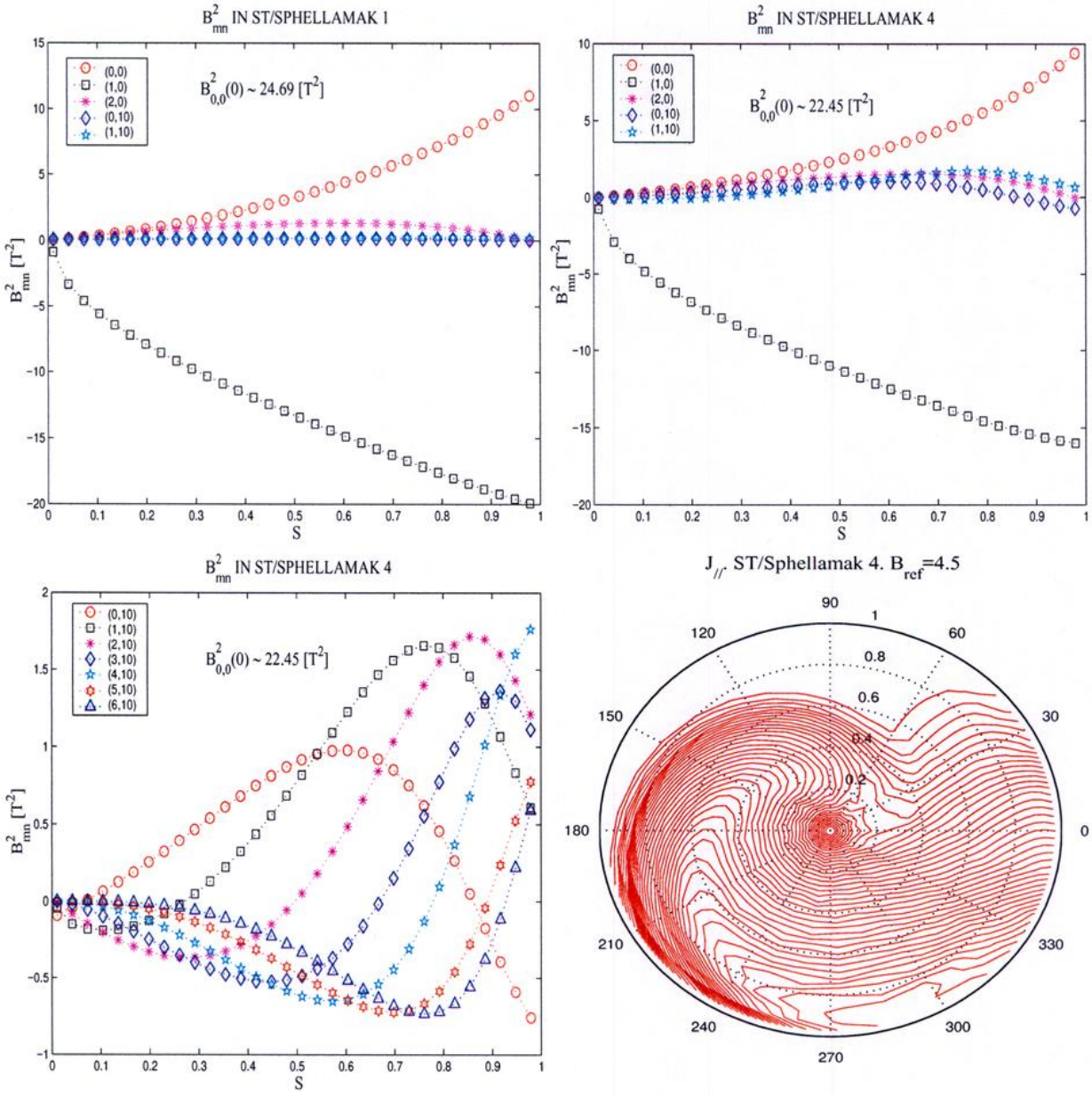
B²mn IN ST/SPHELLAMAK 1
B²0,0(0) ~ 24.69 [T²]
(0,0)
(1,0)
(2,0)
(0,10)
(1,10)
B²mn [T²]
S
B²mn IN ST/SPHELLAMAK 4
B²0,0(0) ~ 22.45 [T²]
(0,0)
(1,0)
(2,0)
(0,10)
(1,10)
B²mn [T²]
S
B²mn IN ST/SPHELLAMAK 4
B²0,0(0) ~ 22.45 [T²]
(0,10)
(1,10)
(2,10)
(3,10)
(4,10)
(5,10)
(6,10)
B²mn [T²]
S
J// ST/Sphellamak 4. Bref=4.5
90
1
120
60
0.8
0.6
150
30
0.4
0.2
180
0
210
330
240
300
270

Figure 4:

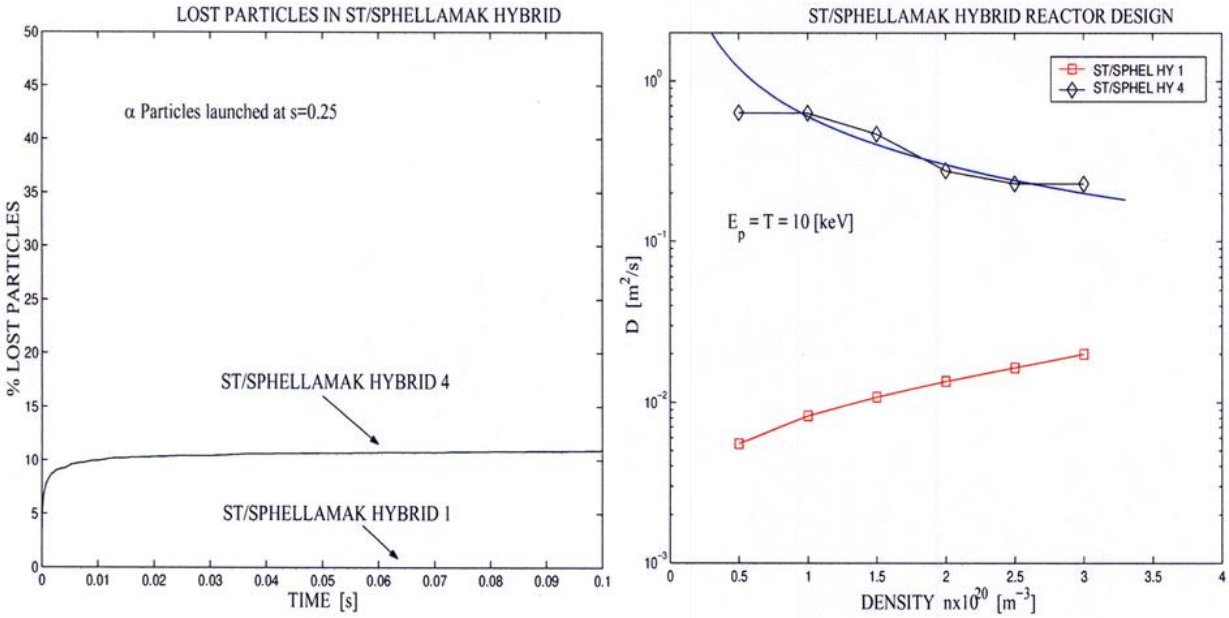
LOST PARTICLES IN ST/SPHELLAMAK HYBRID
α Particles launched at s=0.25
% LOST PARTICLES
TIME [s]
ST/SPHELLAMAK HYBRID 4
ST/SPHELLAMAK HYBRID 1
ST/SPHELLAMAK HYBRID REACTOR DESIGN
ST/SPHEL HY 1
ST/SPHEL HY 4
E_p = T = 10 [keV]
D [m^2/s]
DENSITY nx10^20 [m^-3]

Figure 5:

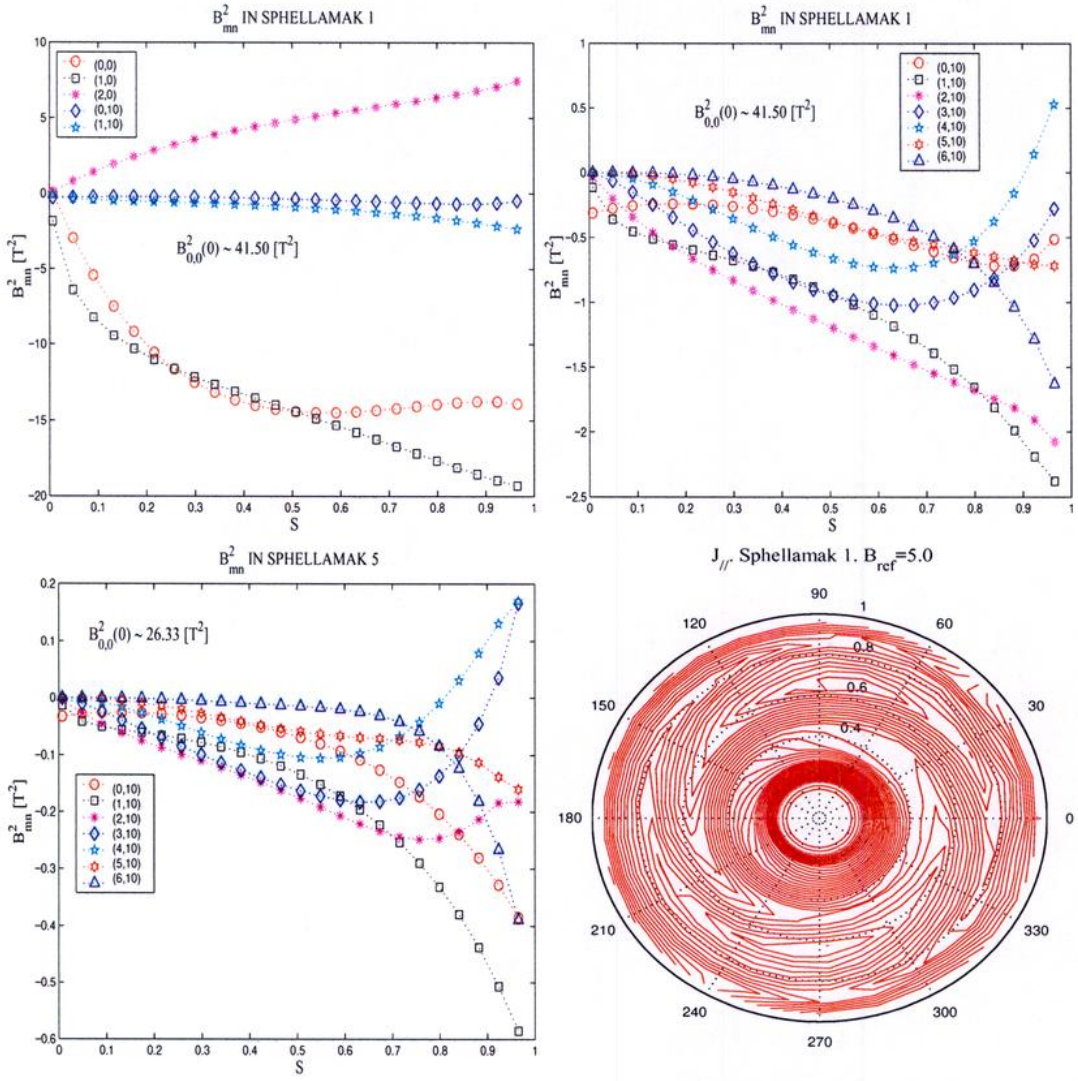
B²mn IN SPHELLAMAK 1
(0,0)
(1,0)
(2,0)
(0,10)
(1,10)
B²0,0(0) ~ 41.50 [T²]
B²mn [T²]
S
B²mn IN SPHELLAMAK 1
(0,10)
(1,10)
(2,10)
(3,10)
(4,10)
(5,10)
(6,10)
B²0,0(0) ~ 41.50 [T²]
B²mn [T²]
S
B²mn IN SPHELLAMAK 5
B²0,0(0) ~ 26.33 [T²]
(0,10)
(1,10)
(2,10)
(3,10)
(4,10)
(5,10)
(6,10)
B²mn [T²]
S
J// Sphellamak 1. Bref=5.0
90
120
60
150
30
180
0
210
330
240
300
270
0.8
0.6
0.4

Figure 6:

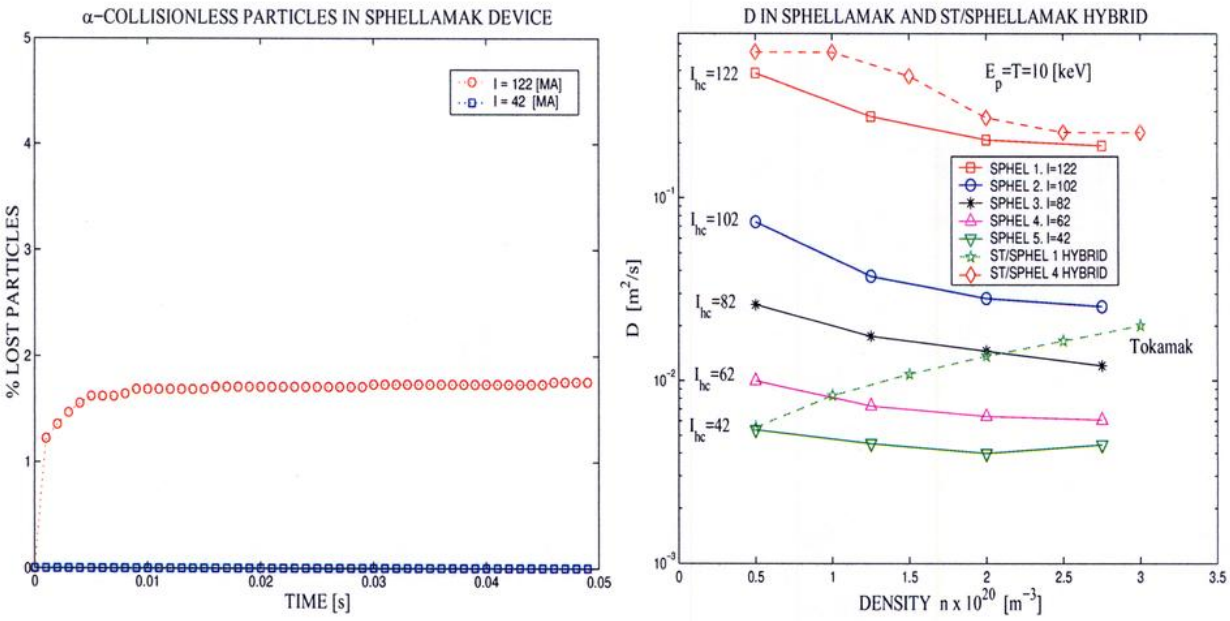
α−COLLISIONLESS PARTICLES IN SPHELLAMAK DEVICE
% LOST PARTICLES
TIME [s]
I = 122 [MA]
I = 42 [MA]
D IN SPHELLAMAK AND ST/SPHELLAMAK HYBRID
D [m²/s]
DENSITY n x 10²⁰ [m⁻³]
E_p=T=10 [keV]
I_hc=122
I_hc=102
I_hc=82
I_hc=62
I_hc=42
SPHEL 1. I=122
SPHEL 2. I=102
SPHEL 3. I=82
SPHEL 4. I=62
SPHEL 5. I=42
ST/SPHEL 1 HYBRID
ST/SPHEL 4 HYBRID
Tokamak

Figure 7:

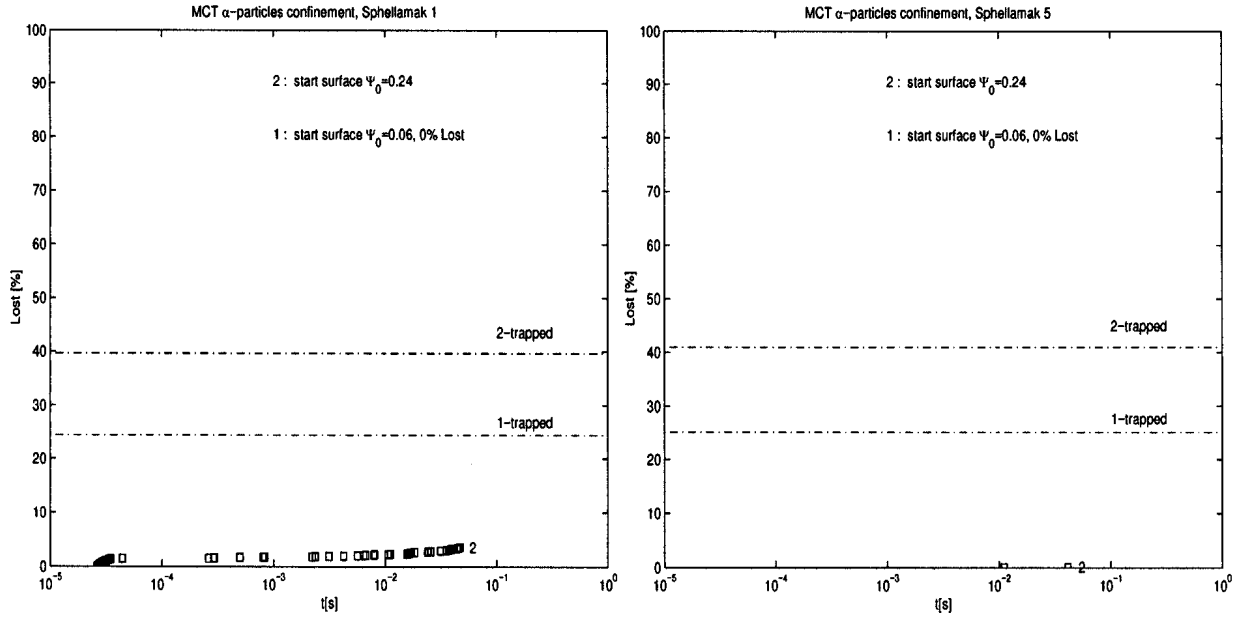
MCT α-particles confinement, Sphellamak 1
2 : start surface Ψ0=0.24
1 : start surface Ψ0=0.06, 0% Lost
2-trapped
1-trapped
Lost [%]
t[s]
MCT α-particles confinement, Sphellamak 5
2 : start surface Ψ0=0.24
1 : start surface Ψ0=0.06, 0% Lost
2-trapped
1-trapped
Lost [%]
t[s]

Figure 8: